Extension of Operating Range of a Centrifugal Compressor by Use of a Non-Axisymmetric Diffuser

ZHENG Xinqian : Ph. D., Tenured Associate Professor, Department of Automotive Engineering, Tsinghua University

LIN Yun : Research Staff, Department of Automotive Engineering, Tsinghua University

KAWAKUBO Tomoki : Manager, Turbomachinery & Engine Technology Department, Product Development Center, Corporate Research & Development

TAMAKI Hideaki : Doctor of Engineering, P. E. Jp, Senior Technical Advisor, Corporate Research & Development

In recent years, higher performance, including higher flow capacities and pressure ratios, is required of the centrifugal compressors used in turbochargers, while compactness is also required in views of improved installability and lower costs. Due to these mutually conflicting requirements, the internal flow velocity tends to increase and the circumferential pressure distortion generated by the non-axisymmetric geometric nature of the discharge scroll gets harsher, and both of these result in the reduction of the stable operating range. In an attempt to overcome this difficulty, a vaneless diffuser with a non-axisymmetric passage geometry has been developed which can suppress the circumferential pressure distortion and consequently retard the occurrence of the destabilizing flow conditions. Performance tests of both the axisymmetric and the non-axisymmetric diffusers confirmed that the non-axisymmetric design can extend the stable flow range by 28% over the conventional axisymmetric design.

1. Introduction

In recent years, for centrifugal compressors used in turbochargers higher performance such as higher flow capacity and pressure ratio has been required, while compactness has also been required in terms of installability and cost. For this reason, a compressor internal passage, and suction and discharge piping have to be laid out in a narrow space, and consequently internal flow velocity and passage curvature are increased, which causes prevention of a higher efficiency and a wider operating range. In particular, circumferential distortion in a flow field caused by non-axisymmetric passages such as a bent suction pipe and a scroll tends to be increasingly enhanced, and the risk of decreasing efficiency and operating range is further increased.

The non-axisymmetry of an internal flow caused by a scroll has been intensively studied so far. The scroll is usually designed to have constant inlet pressure in the circumferential direction at a design point. However, due to its non-axisymmetric geometry, flow passing through the scroll increases in velocity under a high flow rate condition, whereas under a low flow rate condition, it decreases in velocity, causing the circumferential distribution of the scroll inlet pressure[1], [2]. The pressure distribution also reaches the diffuser and the impeller on the upstream side[3], [4], and consequently, the impeller operates under varying conditions. Sorokes et al. have confirmed by experiment that the operation under such varying conditions causes a reduction in performance[5].

Meanwhile, flow field analysis based on Computational Fluid Dynamics (CFD) is also performed. Fatsis et al. have reported, on the basis of three-dimensional unsteady analysis[6], that under the presence of a circumferential pressure distribution on the downstream side of an impeller, the impeller inlet flow angle is no longer constant. Gu et al. have studied the effect of a circumferential pressure gradient on the downstream side of an impeller, and found that when pressure increases in the rotational direction of the impeller, impeller efficiency decreases[7], [8].

The above studies are mainly on subsonic inflow centrifugal compressors; however, in the case of a high pressure ratio centrifugal compressor as focused on in the present study, flow into the impeller or the diffuser is transonic. A flow angle range free from a stall at the leading edge of the impeller decreases in reverse proportion to an inflow Mach number, and therefore the stable operating range of the high pressure ratio centrifugal compressor is expected to be more sensitively affected by non-axisymmetry. Yang et al. have described, through experiments and CFD analysis, that in the case of a high pressure ratio centrifugal compressor, circumferential pressure distortion is more enhanced, and therefore taking account of the effect of the scroll is very important[9]. Zheng et al. have compared the performance of a high pressure ratio centrifugal compressor between under the presence and absence of a scroll using CFD analysis, and obtained the result that the non-axisymmetry of the scroll decreases a stable operating range by up to 42%[10]. Lin et al. have developed an experimental method for evaluating the

effect of the non-axisymmetry of a scroll, and obtained the result that the non-axisymmetry decreases an operating range by 47% and also decreases efficiency by 4.8 points[11].

In order to prevent the non-axisymmetry of a scroll from affecting the upstream side, several methods have been studied. Sorokes et al. have found that by employing a low solidity diffuser, non-axisymmetry becomes unlikely to be transmitted to an impeller[12]. Lin et al. has proposed that not one but multiple discharge passages should be provided to a scroll[11]. The effect of scroll design parameters on a flow field and/or performance has also been studied, and Xu et al. have found that by optimizing the geometry of the tongue area of a scroll, pressure distortion at an impeller outlet can be decreased[13], [14]. Also, an impeller and a passage are ordinarily designed in an axisymmetric geometry; however, Zheng et al. have proposed to cancel the adverse effect of a scroll by purposely designing them in a non-axisymmetric geometry, and by making a casing treatment (a method adapted to expand the operating range of a compressor by extracting flow in the middle of an impeller and returning the extraction to the upstream side of the impeller) non-axisymmetric on the basis of such proposal, succeeded in decreasing a surge flow rate by approximately 10% as compared with a conventional axisymmetric casing treatment[15].

The casing treatment is applied to an impeller part, and therefore of course useless to suppress the non-axisymmetry of a diffuser part. Accordingly, on the basis of the above-described proposal, Zheng et al. have attempted to increase the operating range of the centrifugal compressor by configuring a vaneless diffuser, which is generally an axisymmetric annular passage, in a non-axisymmetric geometry[16]. In this report, we will examine changes in internal flow and operating range on the basis of the experimental and analysis results obtained by Zheng et al.
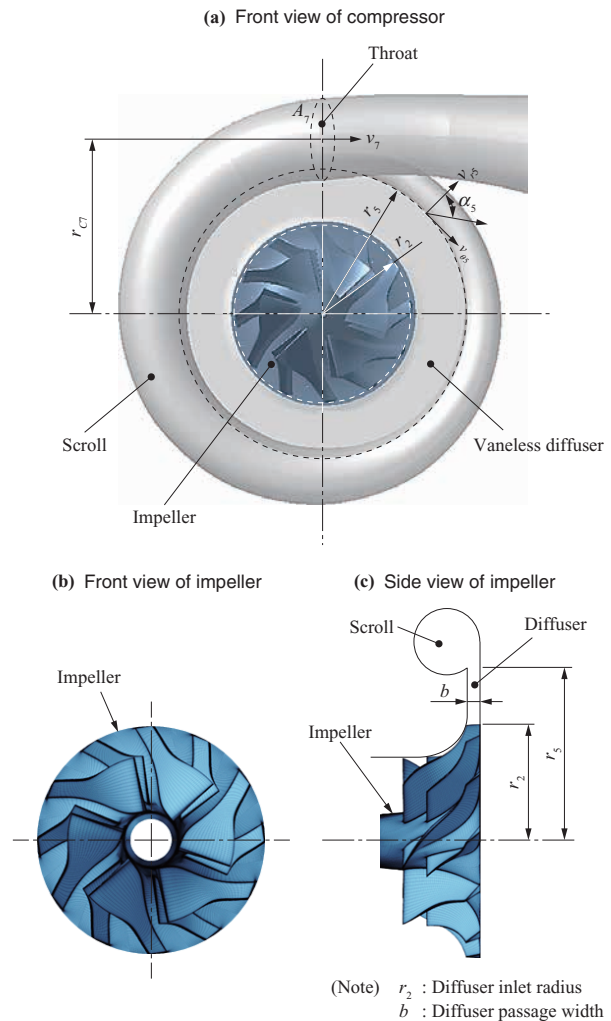
In the following, in **Chapter 2**, we will theoretically examine the occurrence of non-axisymmetric internal flow in a centrifugal compressor under the presence of a scroll and how the non-axisymmetry is transmitted to the upstream side. In **Chapter 3**, we will describe the analysis of the non-axisymmetry of flow by CFD analysis performed on a high pressure ratio test centrifugal compressor, and the examination of an increase in operating range gained by a non-axisymmetric diffuser, and in **Chapter 4**, describe experimental results on a non-axisymmetric diffuser designed on the basis of the results of this examination. Finally, in **Chapter 5**, we will summarize the resulting knowledge.

2. Theoretical discussion

2.1 Occurrence of circumferential pressure distribution by scroll

Figure 1 illustrates a schematic diagram of a test centrifugal compressor, in which main components (impeller, diffuser, and scroll) and the definitions of main dimensions are illustrated. The diffuser treated in the present study is of a vaneless type (vaneless diffuser), which is a type often used in a compressor of a vehicular turbocharger or in a blower.

Conceptionally, the scroll can be regarded as a cascade with

(a) Front view of compressor

(b) Front view of impeller   **(c)** Side view of impeller

(Note)　r_2 : Diffuser inlet radius
　　　　b : Diffuser passage width

Fig. 1　Schematics of test centrifugal compressor

only one blade (= a cascade in which only one passage is present). The passage cross-sectional area of the scroll is designed under a no-load condition (condition where the angular momentum of fluid does not change between the scroll inlet and the throat) as a reference. Under this condition, the circumferential distribution of pressure does not occur at the scroll inlet. The geometry of the scroll is characterized by a parameter referred to as A/R. Here, A represents the cross-sectional area of the throat A_7, and R represents the radius r_{C7} from the center of the impeller to the center of the throat cross section. Under the no-load condition, from the conservation of mass and the conservation of angular momentum, the following equations hold:

$$A_5 v_{r5} = A_7 v_7, \quad \cdots\cdots\cdots\cdots\cdots\cdots\cdots\cdots\cdots(1)$$

and

$$r_5 v_{\theta 5} = r_{C7} v_7, \quad \cdots\cdots\cdots\cdots\cdots\cdots\cdots\cdots\cdots(2)$$

where r_5 and A_5 respectively represent a radius and an annular passage cross section area at the scroll inlet, v_{r5} and $v_{\theta 5}$ a radial velocity and a circumferential velocity at the scroll inlet, and v_7 a velocity at the throat. From Equations (1) and (2), A/R leading to no-load condition under a given scroll inlet condition is given by:

$$(A/R)_{NL} = A_5/\lambda_{r5}, \quad \cdots\cdots\cdots\cdots\cdots\cdots\cdots(3)$$

where $\lambda = \tan\alpha_5$, and α_5 represents an inflow angle to the scroll. Here, the suffix NL represents no-load. A/R of an actual scroll is set to be slightly larger than that under the no-load condition. By applying a slight load at a design point or due to the presence of a tongue having a finite thickness, a pressure distribution occurs to some extent, even at the design point.

On the other hand, at an off-design point, the scroll is burdened with a higher load because of the mismatch between a flow state and a passage geometry as with a usual cascade, thus causing a more enhanced circumferential pressure distribution. With reference to Japikse's sudden expansion loss model[17], a pressure recovery coefficient representing a load from the scroll inlet to the throat is given by

$$C_p = \frac{p_7 - p_5}{p_{05} - p_5} = C_{p\_id} - \zeta_m - \zeta_\theta \quad \cdots\cdots\cdots\cdots\cdots(4)$$

$$C_{p\_id} = 1 - \frac{1}{A_R{}^2\left(1+\lambda^2\right)} \quad \cdots\cdots\cdots\cdots\cdots\cdots(5)$$

$$\zeta_m = \frac{1}{1+\lambda^2} \quad \cdots\cdots\cdots\cdots\cdots\cdots\cdots(6)$$

$$\zeta_\theta = \begin{cases} \dfrac{\left(\lambda A_R / R_R - 1\right)^2}{A_R{}^2\left(1+\lambda^2\right)} & \left(\dfrac{\lambda A_R}{R_R} \geq 1\right) \\[4mm] 0 & \left(\dfrac{\lambda A_R}{R_R} \leq 1\right), \end{cases} \quad \cdots\cdots\cdots\cdots(7)$$

where C_p: pressure recovery coefficient, p_5: scroll inlet static pressure, p_7: scroll throat part static pressure, and p_{05}: scroll inlet total pressure. Also, C_{p_id} represents a loss free ideal pressure recovery, ζ_m a radial loss, and ζ_θ a circumferential loss. Further, $A_R = A_7/A_5$ and $R_R = r_{C7}/r_5$. The loss ζ_θ becomes zero under the no-load condition $(A/R)/(A/R)_{NL} = \lambda A_R/R_R = 1$, and C_p also becomes zero near the no-load condition. By using this model, the degree of pressure distortion at the scroll inlet at the off-design point can be estimated. Also, Iversen et al. and Chochua et al. have proposed a method for obtaining a circumferential pressure distribution by applying conservation laws in a flow direction inside a scroll passage as a more detailed model[18], [19].

These models can specifically estimate the degree of pressure distortion on the basis of scroll geometry although they assume that the flow in the upstream side of a scroll is axisymmetric.

2.2 Reductions in efficiency and stable operating range due to non-axisymmetry

The stable operating limit of a centrifugal compressor on a low flow rate side is determined by the occurrence of fluid self-excited oscillation called a surge in the entire piping system including the compressor. Such a surge phenomenon is strongly related to the pressure rise capability of the compressor, and likely to appear when the pressure rise capability is reduced due to the occurrence of a boundary layer separation and/or a reverse flow inside the compressor and/or when flow is irreversibly broken up. **Figure 2** illustrates schematic diagrams of an internal flow of the centrifugal compressor at a design flow rate and at a very low flow rate.

(a) Operation at appropriate flow rate

Forward flow in main flow

Forward flow in boundary layer

Impeller blade

(b) Operation at very low flow rate

Forward flow in main flow

Reverse flow in boundary layer

Impeller blade
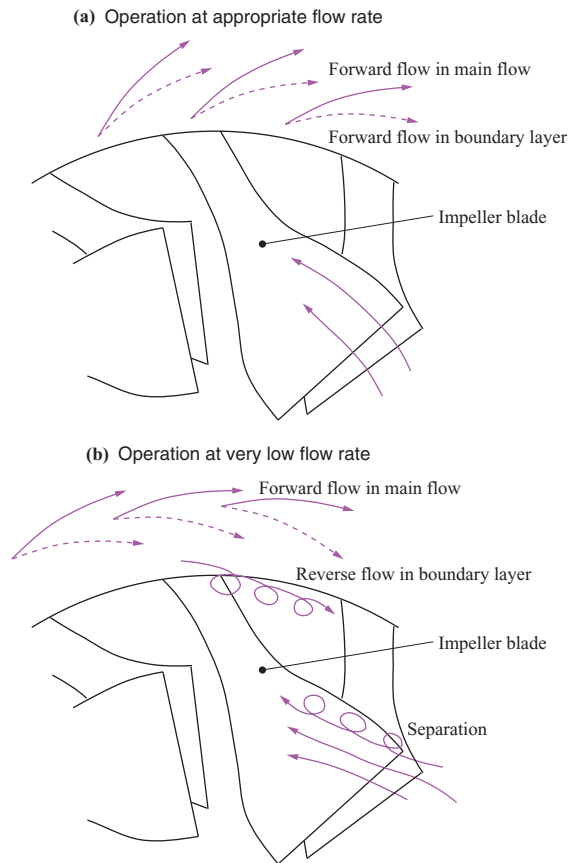
Separation

Fig. 2 Schematics of internal flow in centrifugal compressor

For example, at an operating point on the low flow rate side, flow into the impeller is not aligned to a direction of the blades, and therefore likely to separate and/or stall at the fore ends of the blades. Also, at the operating point on the low flow rate side, a radially outward velocity component inside the diffuser decreases. As a result, fluid having less momentum inside the boundary layer cannot withstand a radial pressure rise, and is likely to flow backward and/or stall. Such separation and/or reverse flow in the boundary layer cause a pressure loss and narrow the passage, thus retarding or decreasing the pressure rise capability of the compressor. Further, when the reverse flow from the diffuser gets into the impeller on the upstream side, the pressure rise capability of the impeller is immediately lost. The occurrence and progress of such phenomena make the surge phenomenon likely to occur.

When the impeller and the diffuser operate under circumferentially uniform conditions, the separation and/or the reverse flow do not occur at any specific circumferential position; however, when the flow is not circumferentially uniform due to some causes such as the scroll and inlet distortion, the separation and/or the reverse flow occur first at the worst conditioned position. Therefore, when there is circumferential variation, the surge is more likely to occur. Also, as the pressure ratio and efficiency of the compressor draw upward convex curves with respect to the flow rate, the pressure ratio and the efficiency take average values of those corresponding to different flow rates and, as a result, inevitably

take lower values than those without circumferential variation. Therefore, in order to make full use of the potential of the intrinsic compressor capability in the pressure ratio, efficiency, and operating range, the non-axisymmetry caused by the scroll and the like must be kept as low as possible.

2.3 Pressure disturbance in vaneless diffuser

Our experience tells us that a pressure disturbance caused by an object placed in a flow decays with distance from the object (distance decay). However, in the case of a radial passage like the vaneless diffuser of the centrifugal compressor, the situation is a bit more complicated. This can also be analogically understood from the fact that when a cylindrical wave propagates toward the center, its amplitude increases. **Figure 3** illustrates an axisymmetric annular passage, and we will examine a flow in an axial passage (**Fig. 3-(a)**) and a flow in a radial passage (**Fig. 3-(b)**) comparing each other. First, the conjugate complex velocity in the axial passage:

$$W = W_0\left(e^{-i\alpha} + \varepsilon e^{Z/r_0}\right) \quad \cdots\cdots\cdots\cdots(8)$$

e : The base of natural logarithm
i : The imaginary unit
ε : Small amplitude

represents the situation where a circumferential (Y directional) periodic disturbance superposed on a uniform flow having a velocity of W_0 and a flow angle of α decays toward the upstream side (in the $-X$ direction). Mapping this onto the radial passage using a conformal mapping transformation $Z = r_0\ln(z/r_0)$ gives:

$$w = \left(dZ / dz\right)W = W_0\left(r_0 e^{-i\alpha} / z + \varepsilon\right). \quad \cdots\cdots\cdots(9)$$

The left half plane of the Z plane before the mapping is mapped inside a circle having a radius r_0 in the z plane after the mapping, and the latter just schematically represents a
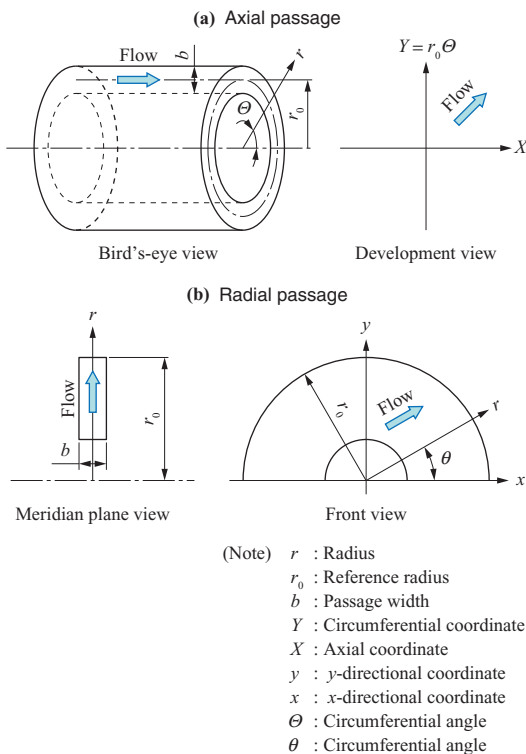
situation where a disturbance at a scroll inlet propagates toward an upstream side. Pressure fields corresponding to these cases are respectively given using the Bernoulli's theorem by:

$$\frac{p_0 - p}{\rho W_0^2 / 2} = 1 + 2\varepsilon e^{X/r_0}\cos\left(\Theta + \alpha\right) + \varepsilon^2 e^{2X/r_0}, \quad \cdots\cdots(10)$$

and

$$\frac{p_0 - p}{\rho W_0^2 / 2} = \left(\frac{r_0}{r}\right)^2 + 2\varepsilon\frac{r_0}{r}\cos\left(\theta + \alpha\right) + \varepsilon^2, \quad \cdots\cdots(11)$$

where

Θ: Circumferential angle in Z plane
θ : Circumferential angle in z plane.

Here, p_0 represents the total pressure, p the static pressure, and ρ the density. **Figure 4** illustrates static pressure distributions due to potential flows in the axisymmetric annular passages, in which **-(a)** illustrates the static pressure distribution in the axial passage and **-(b)** illustrates the static pressure distribution in the radial passage. The circumferential pressure disturbance represented by the second term on the right side of Equation (10) for the axial flow case exponentially decays toward the upstream side as expected, whereas that represented by the second term on the right side of Equation (11) for the radial flow case is amplified toward the upstream side.
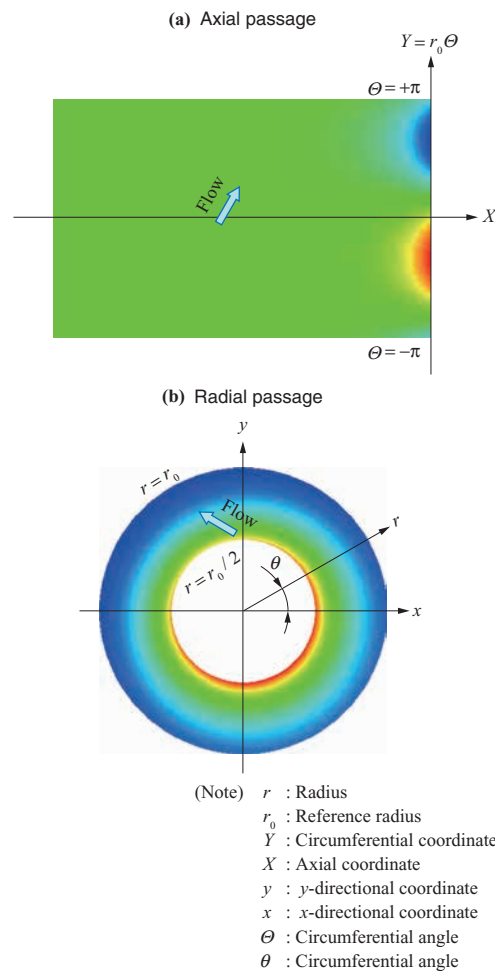

(a) Axial passage

(b) Radial passage

(Note) r : Radius
r_0 : Reference radius
Y : Circumferential coordinate
X : Axial coordinate
y : y-directional coordinate
x : x-directional coordinate
Θ : Circumferential angle
θ : Circumferential angle

Fig. 4   Pressure distribution of potential flow in axisymmetric annulus passage

(a) Axial passage

Bird's-eye view   Development view

(b) Radial passage

Meridian plane view   Front view

(Note) r : Radius
r_0 : Reference radius
b : Passage width
Y : Circumferential coordinate
X : Axial coordinate
y : y-directional coordinate
x : x-directional coordinate
Θ : Circumferential angle
θ : Circumferential angle

Fig. 3   Axisymmetric annulus passages

Such situations will be examined in more detail using the linear theory. It is assumed that the flow is a two-dimensional, steady, incompressible, and inviscid one in the axisymmetric annular passages having a constant thickness as illustrated in **Fig. 3**, in which a non-axisymmetric infinitesimal disturbance is assumed to be superposed on an axisymmetric mean flow. When the circumferential disturbance is expressed by a kth sinusoidal wave, pressure disturbances in the axial and radial passages are, with reference to References (20) and (21), given by:

$$p(X, \Theta) = \left(A e^{kX/r_0} + B e^{-kX/r_0} \right) e^{ik\Theta}, \quad \cdots\cdots\cdots\cdots(12)$$

and

$$p(r, \theta) = \left(A r^{k-2} + B r^{-k-2} + C r^{-ik\lambda} \right) e^{ik\theta}, \quad \cdots\cdots\cdots(13)$$

respectively.

Here, $\lambda = \tan\alpha$, and under current assumptions, λ takes a constant value. The first and second terms on the right sides represent an irrotational flow, and as with the previous example of the potential flow, in the axial passage, it changes exponentially whereas in the radial passage, it changes as a power function. The third term of Equation (13) the case of the vaneless diffuser, it is a component generated due to the uneven blade-to-blade loadings in the circumference of the impeller. This term can also be expressed by $r^{-ik\lambda} e^{ik\theta} = e^{ik(\theta - \lambda \ln r)}$ and therefore its value is constant along a logarithmic spiral $\theta - \lambda \ln r = $ const. which represents the stream line of the axisymmetric mean flow.

The coefficients A, B, and C are determined by boundary conditions. We will now examine how, on the assumption that a pressure distortion of $p(r_5, \theta) = P_5 e^{ik\theta}$ is given at the scroll inlet, the pressure distortion is amplified or decayed inside the vaneless diffuser. The boundary conditions at the diffuser inlet are determined by impeller characteristics, and therefore cannot be easily given; however, they can be generally expressed by the following equations anyway.

$$P_2 / \rho \bar{v}_{r2} = -Z V_{r2}, \quad V_{\theta 2} = \Lambda V_{r2} \quad \cdots\cdots\cdots\cdots(14)$$

Here, ρ represents the density, $\bar{v}_{r2}$ the circumferential average of the radial velocity at the diffuser inlet, P, V_r, V_θ the complex amplitudes representing the disturbances of pressure, radial velocity, and circumferential velocity, respectively, and the suffixes "2" and "5" the diffuser inlet and outlet. Z and Λ are complex numbers determined by the impeller characteristics. In the following, as the boundary conditions for the determination of them, three cases (Equations (15) to (17) below) are considered. As the simplest case, if the total pressure and absolute flow angle are assumed to be uniform at the impeller outlet, Equation (15) holds.

$$P_2 / \rho \bar{v}_{r2} + V_{r2} + \lambda V_{\theta 2} = 0, \quad V_{\theta 2} = \lambda V_{r2}$$
$$Z = 1 + \lambda^2, \quad \Lambda = \lambda \quad \cdots\cdots\cdots\cdots\cdots(15)$$

This is rather an unrealistic condition. As a more realistic condition, if we consider an ideal impeller with no loss and constant relative outlet flow angle, Equation (16) holds.

$$P_2 / \rho \bar{v}_{r2} + V_{r2} + \lambda_R V_{\theta 2} = 0, \quad V_{\theta 2} = \lambda_R V_{r2}$$
$$Z = 1 + \lambda_R^2, \quad \Lambda = \lambda_R \quad \cdots\cdots\cdots\cdots(16)$$

Here $\lambda_R = \tan\beta_2$, and β_2 represents an impeller relative outlet flow angle. These conditions are based on the assumption that each blade-to-blade passage responses to a variation in back pressure in a quasi-steady manner. As yet another case, if one can predict the impeller performance at two close flow rates by means of one-dimensional analysis or CFD analysis, one can use the small differences between these solutions as Equation (17).

$$Z = -\Delta p_2 / (\rho v_{r2} \Delta v_{r2}), \quad \Lambda = \Delta v_{\theta 2} / \Delta v_{r2} \quad \cdots\cdots\cdots(17)$$

Here, Δ represents the difference between impeller outlet state quantities (pressure p_2, radial velocity v_{r2}, circumferential velocity $v_{\theta 2}$). Since these boundary conditions are based on the quasi-static assumption, Z and Λ are purely real numbers; however, in fact, they should include imaginary parts corresponding to a phase delay, respectively. Also, Equations (16) and (17) are based on the implicit assumption that the impeller inlet state is uniform; however, the physically irrelevant component, similar to the second term of Equation (12), that increases toward the upstream side should be removed.

Among the above-described three sets of boundary conditions, the solution of Equation (15) can be relatively simply expressed by

$$P_2 / P_5 = 2 / \{ (r_5/r_2)^{k-2} + (r_5/r_2)^{-k-2} \}. \quad \cdots\cdots\cdots\cdots(18)$$

In this case, an amplification factor does not depend on the flow angle. Also, since no imaginary part is included, the circumferential distribution does not have any phase shift between the inlet and the outlet. The solutions of the other cases corresponding to Equations (16) and (17), can also be expressed in a similar manner, but are omitted here because of their complexity.

Figure 5 illustrates an amplitude ratio and a phase difference of a pressure disturbance modes inside the diffuser, in which the solutions corresponding to the three cases are illustrated at each of the first to sixth circumferential wavenumbers. A flow field considered here is the diffuser of the centrifugal compressor studied in the next section. In any cases, the first three modes have the amplification factor close to or greater than 1, which seems to significantly affect the impeller and/or the diffuser in terms of their stalls. **Figure 5** also illustrates a resonance-like feature where the phases suddenly change around the wavenumber giving the maximum amplitudes in Equations (16) and (17). In the fourth or higher mode, the amplification factor is small, and also spectrum amplitude at the scroll inlet is essentially small, so their effect may be ignored. Further, in a mode higher than the sixth mode, the validity of the assumption of the quasi-steady impeller response may be low.

As is clear from the above, inside the vaneless diffuser, the simple distance decay of pressure nonuniformity caused by the scroll cannot necessarily be expected, and therefore a method for suppressing the effect of non-axisymmetry in some way is demanded.

3. Design of non-axisymmetric vaneless diffuser

3.1 Numerical analysis method

The main specifications of the test centrifugal compressor as a base are listed in **Table 1**. Also, **Fig. 6** illustrates the test centrifugal compressor. The cross-sectional geometry of the
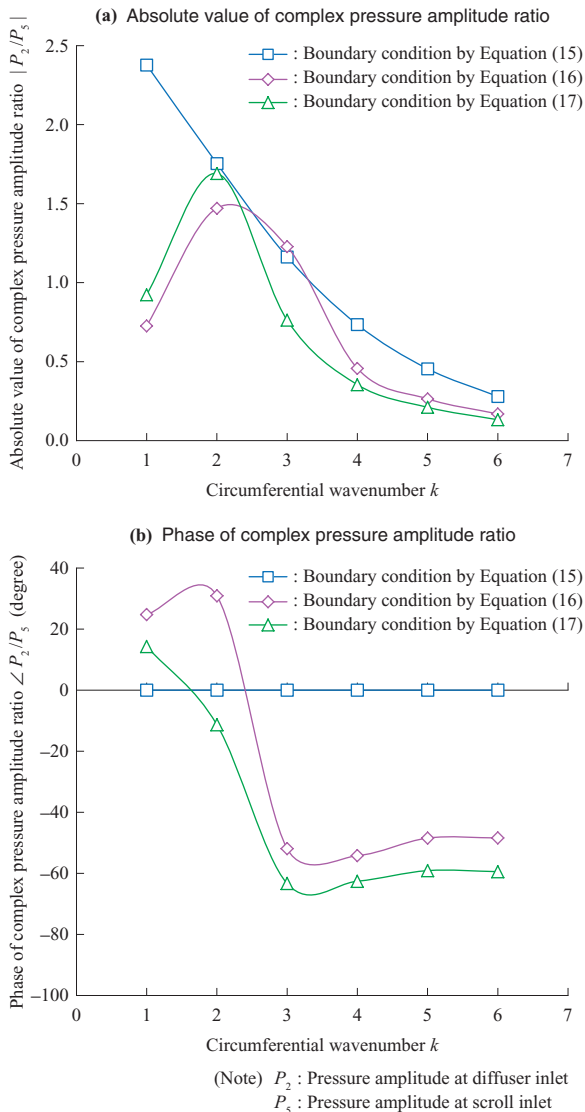
(a) Absolute value of complex pressure amplitude ratio

Legend:
- □ : Boundary condition by Equation (15)
- ◇ : Boundary condition by Equation (16)
- △ : Boundary condition by Equation (17)

x-axis: Circumferential wavenumber k
y-axis: Absolute value of complex pressure amplitude ratio $|P_2/P_5|$

(b) Phase of complex pressure amplitude ratio

Legend:
- □ : Boundary condition by Equation (15)
- ◇ : Boundary condition by Equation (16)
- △ : Boundary condition by Equation (17)

x-axis: Circumferential wavenumber k
y-axis: Phase of complex pressure amplitude ratio $\angle P_2/P_5$ (degree)

(Note) P_2 : Pressure amplitude at diffuser inlet
P_5 : Pressure amplitude at scroll inlet

Fig. 5 Amplitude ratio and phase difference of modal pressure disturbance in diffuser

Table 1 Main parameters of test centrifugal compressor

Parameter	Symbol	Unit	Value
Design pressure ratio	π	—	4.0
Design rotor speed	N	rpm	170 000
Design mass flow rate	$\dot{m}$	kg/s	0.24
Impeller inlet diameter	D_{1s}	mm	40.9
Impeller outlet diameter	D_2	mm	62.15
Impeller outlet blade height	b_2	mm	4.1
Impeller backward angle	β_{b2}	degree	−31.5
Number of impeller blades	Z_b	—	6 + 6 (long blades + short blades)
Diffuser outlet diameter	D_5	mm	100
Diffuser passage height	b	mm	3.13
Scroll A/R	A/R	mm	11.2
Scroll throat area	A_7	mm²	632

scroll passage is nearly circular (ellipsoidal), and the scroll is designed such that pressure at the scroll inlet is nearly uniform in the circumferential direction at a design point.
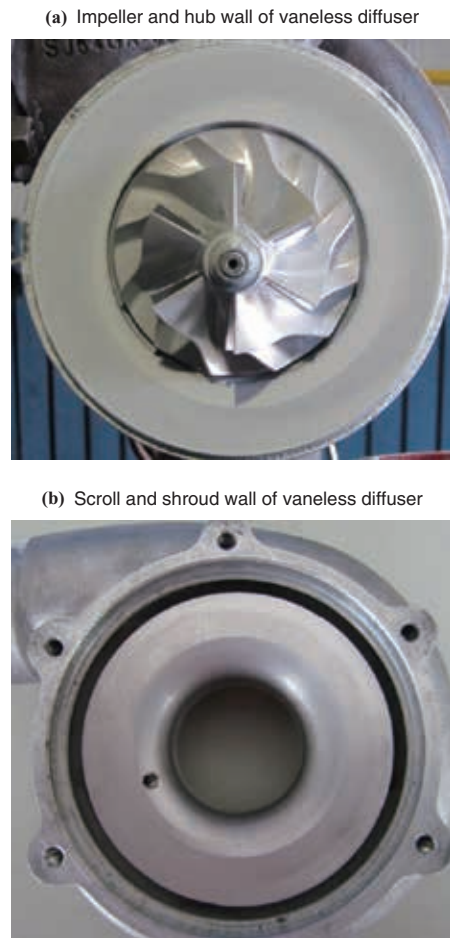
In order to examine the internal flow of the vaneless

(a) Impeller and hub wall of vaneless diffuser

(b) Scroll and shroud wall of vaneless diffuser

Fig. 6 Test centrifugal compressor

diffuser in detail to obtain basic data and a design guideline for designing non-axisymmetric diffusers, the CFD analysis is performed on the entire centrifugal compressor. As a CFD solver, FINE™/Turbo of NUMECA International (Belgium) is used. This is a solver adapted to solve 3D compressible Reynolds-averaged Navier-Stokes equations using a finite volume method. The space derivative is discretized using central differences, and time-integrated using the fourth-order Runge-Kutta method. As a turbulence model, the one-equation Spalart-Allmaras model is used. The domain connection between moving and stationary blades is based on the Frozen Rotor model. The connecting interface is located at 1.03 times the impeller outlet diameter.

The total number of cells is set to approximately 6.3 million (cells) on the basis of grid dependency test results. A grid model to be used satisfies all criteria such as an orthogonality of 13.3° or more, a grid width growing rate of 5 or less in the boundary layer, an aspect ratio of 1 000 or less. The first grid width y^+ in the boundary layer is suppressed to 5 or less.

As the boundary conditions, at the inlet boundary, total pressure, total temperature, and flow angle are given, and at the outlet boundary, static pressure is given. On the solid wall, adiabatic and no-slip conditions are imposed.
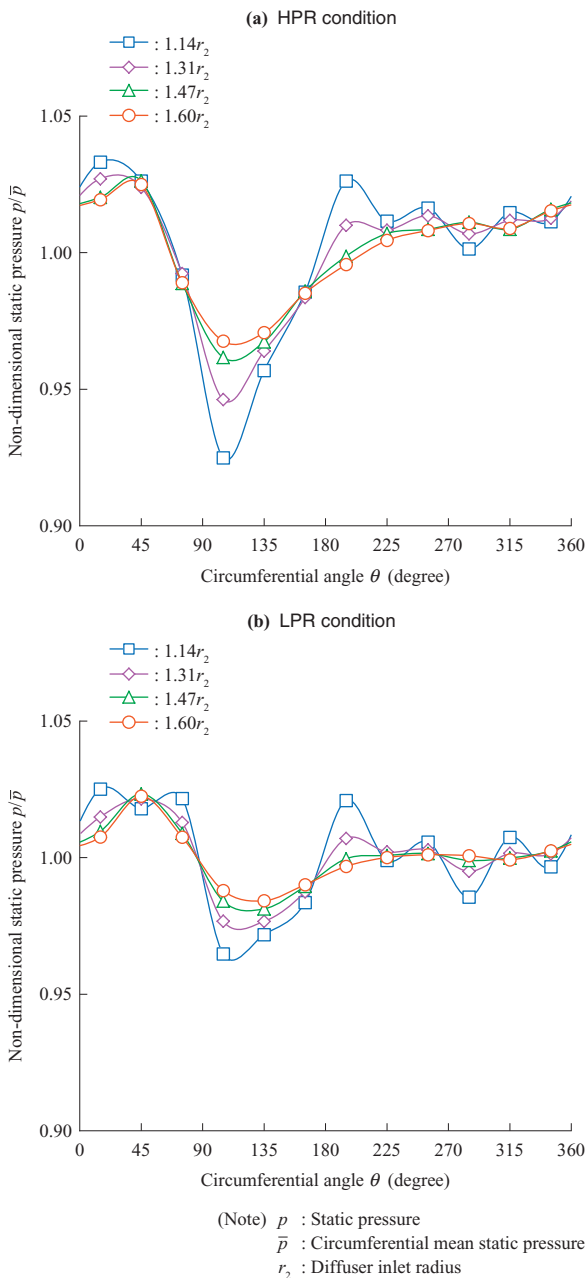
For information on the validation of the overall performance prediction accuracy of the CFD analysis, see Reference (14).

3.2 Analysis results on axisymmetric diffuser

First, we will examine analysis results on a compressor having an axisymmetric diffuser (hereinafter referred to as a base configuration). The analysis results on a surge side under a High Pressure Ratio (HPR) condition (a rotor speed of 170 000 rpm) and under a Low Pressure Ratio (LPR) condition (a rotor speed of 120 000 rpm) will be examined.

(1) Static pressure distribution in diffuser

Figure 7 illustrates circumferential static pressure distributions in the diffuser near surge points, in which the circumferential static pressure distributions at four radial positions from the inlet to outlet of the diffuser under the HPR condition (**Fig. 7-(a)**) and under the LPR condition (**Fig. 7-(b)**) are illustrated. All pressure values are normalized to mean static pressures at the respective radial positions. As expected, the pressures are not uniform in the circumferential direction, and in any of the conditions, a pressure drop is found around a circumferential angle of 105°. Yang et al. has compared the nonuniformity of static pressure between experiment and CDF and confirmed that even steady analysis using the Frozen Rotor model can predict such distributions with sufficient accuracy[9].
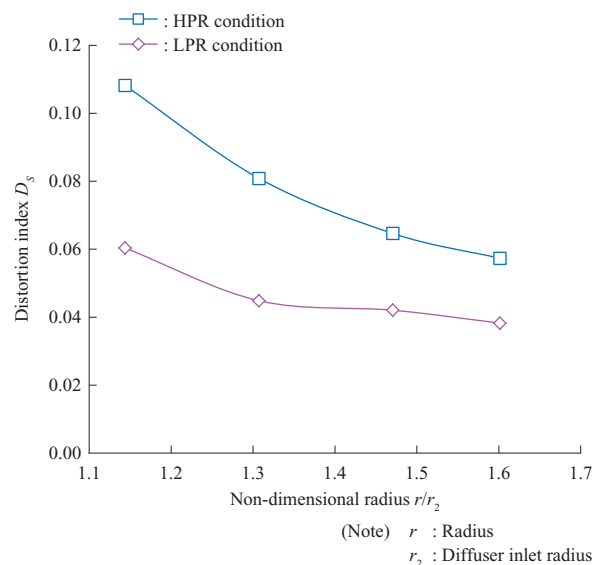
In the following discussion, as an index for the circumferential nonuniformity in the pressure distributions, a distortion index defined by the following equation is used.

$$D_s = (p_{max} - p_{min}) / \bar{p} \quad \text{.............................(19)}$$

Here, p_{max}, p_{min}, $\bar{p}$ represent the maximum, minimum, and mean values of pressure at a certain radial position, respectively. **Figure 8** illustrates the distortion index in the diffuser near the surge point. From **Fig. 8**, it turns out that the pressure distortion is more noticeable under the HPR condition than under the LPR condition. Also, in either case, the pressure distortion is enhanced from the diffuser outlet toward the upstream side. Such situations have also been reported in the experimental results of Reference (9).

Calculating the distortion index at the scroll inlet under the HPR condition using previously shown Equation (4) results in 0.074, which is larger than 0.057 derived from a CFD analysis result but still in a similar order. In this case, $r_{C7} > r_5$; however, Equation (4) does not take account of pressure difference due to the radius difference, and therefore should give a bit higher pressure. Estimating the pressure difference on the assumption of radial equilibrium gives the following equation.

$$\Delta C_p \sim \frac{\rho \left(v_7^2 / r_{C7} \right) \left(r_5 - r_{C7} \right)}{p_{05} - p_5} = \frac{2 \left(1 / R_R - 1 \right)}{A_R^2 \left(1 + \lambda^2 \right)} \quad \text{.......(20)}$$

(a) HPR condition

(b) LPR condition

(Note) p : Static pressure
$\bar{p}$: Circumferential mean static pressure
r_2 : Diffuser inlet radius

Fig. 7 Circumferential pressure distribution in diffuser at near-surge conditions

(Note) r : Radius
r_2 : Diffuser inlet radius

Fig. 8 Distortion index in diffuser at near-surge conditions

Correcting the calculated distortion index using Equation (20) results in 0.062, which is a value close to the CFD analysis result.

Figure 9 illustrates an amplitude ratio and phase difference at each circumferential wavenumber mode of a pressure disturbance mode in the diffuser. Around a wavenumber of 2 or 3, the peak of the amplitude ratio is present, and a situation where the positive and negative of the phase difference are switched around these wavenumber substantially agrees with the linear theory calculation results illustrated in **Fig. 5** (in the cases of the sets of boundary conditions given by Equation (16) or (17)).

(2) Mach number distribution in diffuser

Figure 10 illustrates Mach number distributions near the surge points under the HPR condition and under the LPR condition, in which Mach numbers inside the diffuser at 10, 50, and 90% span cross sections under the HPR condition (**Fig. 10-(a)**) and under the LPR condition (**Fig. 10-(b)**) are illustrated. From **Fig. 10**, a situation where a jet-wake structure from the impeller traverses and decays inside the diffuser can be seen. Also, it turns out that under any of the HPR condition and the LPR condition, momentum on the shroud side is lower than those on the hub side and on the mid-passage section. This suggests that reverse flow in the

(a) Absolute value of complex pressure amplitude ratio

(b) Phase of complex pressure amplitude ratio

(Note) P_2 : Pressure amplitude at diffuser inlet
P_5 : Pressure amplitude at scroll inlet

Fig. 9 Amplitude ratio and phase difference of modal pressure disturbance in diffuser

(a) HPR condition

10% span 50% span 90% span

(b) LPR condition

10% span 50% span 90% span

Fig. 10 Mach number distribution at HPR and LPR near-surge conditions

vaneless diffuser is highly likely to occur first on the shroud side.

### 3.3 Design guideline for non-axisymmetric diffusers

In the centrifugal compressor, either the stall of the impeller or the stall of the diffuser may act as a trigger for the surge; however, usually, under a high pressure ratio condition, the impeller stall is more likely to cause the surge. Under the high pressure ratio condition, the impeller flow is sensitive to non-axisymmetry[9]-[11], [15], and some blade-to-blade passages are exposed to more adverse conditions than the other blade-to-blade passages, and a stall in such an adversely conditioned passage is expected to act as a trigger for the surge. The circumferentially uneven operation of the impeller is caused by the non-axisymmetry of pressure on the downstream side of the impeller, and therefore if such a pressure distribution can be suppressed by taking some sort of means, it may be possible to delay the stall of the impeller.

On the other hand, under the low pressure ratio condition, the diffuser stall often acts as a trigger for the surge. This can also be confirmed from the below-described experimental results. A stall in the vaneless diffuser may be caused by reverse flow near the wall. When the flow field of the vaneless diffuser is made non-axisymmetric by the effect of the scroll, reverse flow may first occur in a position where a flow state is the worst on the circumference. If the non-symmetry can be suppressed by taking some sort of means, it may be possible to delay the stall of the diffuser.

Therefore, the purpose of designing the non-axisymmetry diffuser is to improve the stability of the compressor by configuring the diffuser in a non-axisymmetric geometry to thereby keep the non-axisymmetry caused by the scroll as low as possible. In the base configuration, the pressure is minimized at a circumferential position of 105°. When expanding the passage width of the diffuser at this circumferential position, the circumferential static pressure distribution of the diffuser may be made more uniform because of the deceleration of the flow, and the internal flow of the impeller and the diffuser may get closer to an axisymmetric flow. Accordingly, the basic design guideline for axisymmetric diffusers is to widen (narrow) the passage height of the diffuser at a circumferential position where the static pressure is low (high).

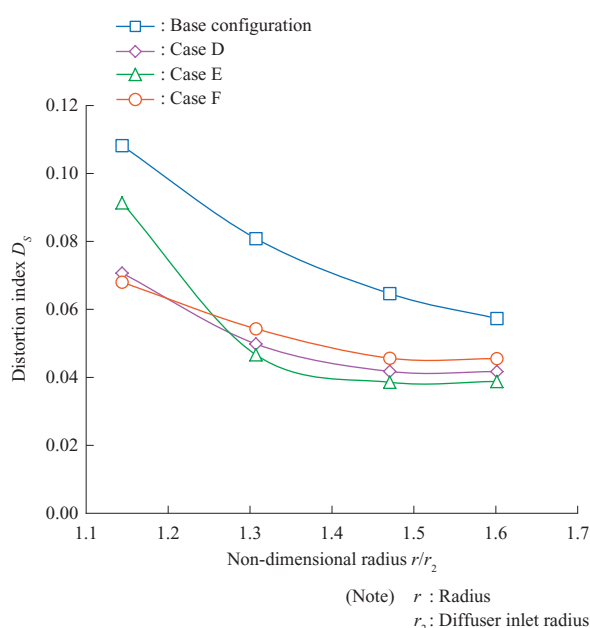### 3.4 Design of non-axisymmetric diffuser

On the basis of the above-described design guideline for non-axisymmetric diffusers, non-axisymmetric diffusers having three different passage width distributions have been designed. **Figure 11** illustrates the passage width distributions. In any of the cases, a radial diffuser passage width is constant from the diffuser inlet ($1.126r_2$) to the diffuser outlet ($1.61r_2$), and a circumferential distribution is such that at a position of 105° where the diffuser of the base configuration exhibits the lowest pressure, a passage flow width is maximized. In any of the cases, the circumferential mean value of the passage width is the same as that in the base configuration. A change in passage width distribution is made only by changing a shroud wall, and the hub wall remains the same as that in the base configuration. Also, the shroud wall forming a pinch
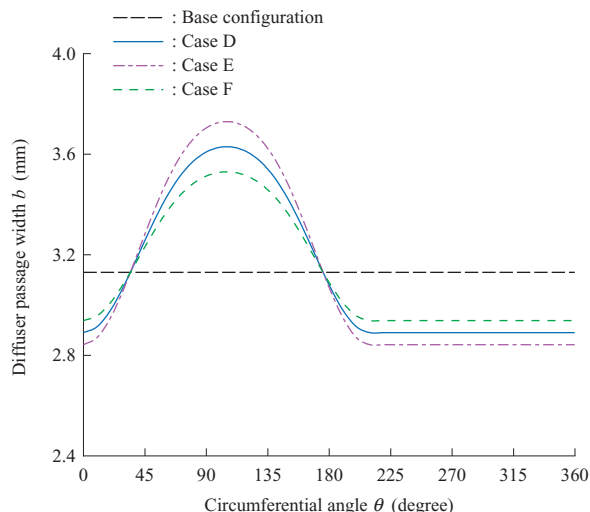
Fig. 11 Passage width distribution of diffusers

geometry (contracted flow part) between the impeller outlet and the diffuser inlet smoothly changes from an axisymmetric geometry to a non-axisymmetric geometry. The shroud wall in the impeller part is the same as that in the base configuration.
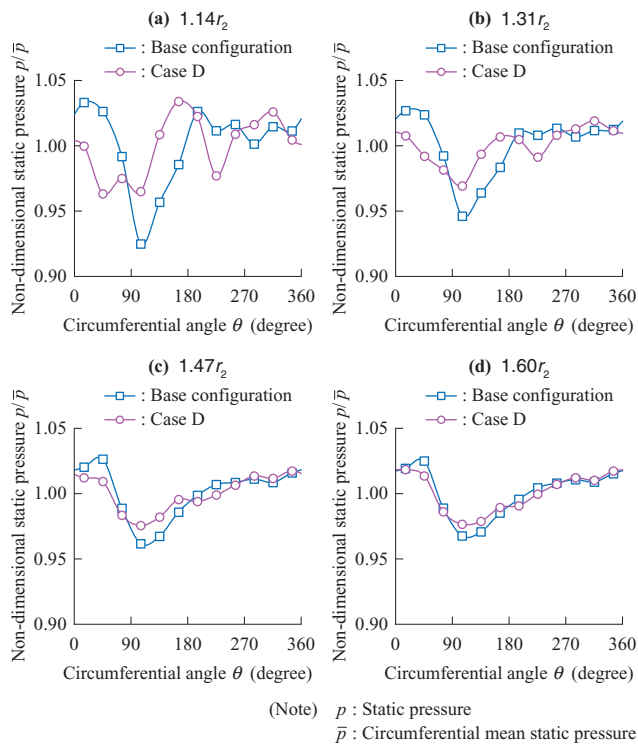
Figure 12 illustrates distortion indices in the diffusers around a surge point under the HPR condition, in which pressure distortions in the three cases obtained by the CFD analysis under the HPR condition are illustrated together with the base configuration. As compared with the pressure distortion in the base configuration, in any of the three cases, the pressure distortion is greatly suppressed. In the case E where the degree of geometric non-axisymmetry is the highest, the degree of non-axisymmetry is most suppressed on the outer circumferential side, whereas at the diffuser inlet, the degree of non-axisymmetry is higher than those in the other two configurations. The case F where the degree of geometric non-axisymmetry is the lowest exhibits a tendency
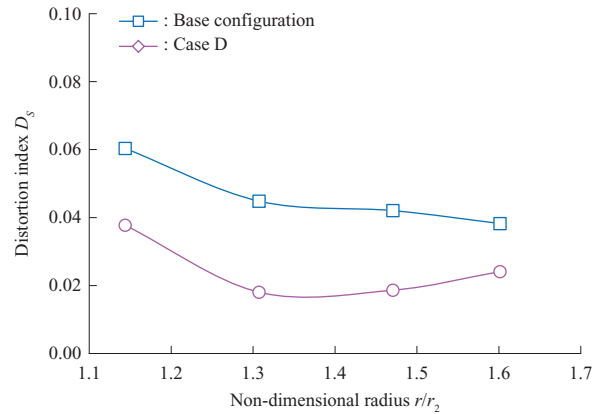

(Note) r : Radius
r_2 : Diffuser inlet radius

Fig. 12 Distortion index in diffuser at HPR near-surge conditions

opposite to the case E. The reciprocal relationship between the outer circumferential side and the inner circumferential side may be related to the fact that as illustrated in **Fig. 10**, the supersonic flow is formed at the impeller outlet. In general, a supersonic flow increases in velocity and decreases in pressure as a passage is expanded, whereas a subsonic flow exhibits the opposite tendency. The above-described design guideline for non-axisymmetric diffusers is effective only for a subsonic flow range that covers most of the diffuser.

Accordingly, it is necessary to optimize the geometry also in consideration of the fact that a supersonic flow is formed on the diffuser inlet side. From **Fig. 12**, it is considered that the case D can form the best pressure field. **Figure 13** illustrates circumferential static pressure distributions in the diffusers near the surge point under the HPR condition, in which the circumferential static distribution is compared between the base configuration and the case D. In the case D, it turns out that on the inner diameter side (**Figs. 13-(a)** and **-(b)**), the pressure distortion is considerably suppressed. **Figure 14** illustrates the pressure distortions in the base configuration and in the case D under the LPR condition. Further, **Fig. 15** illustrates a comparison of a circumferential static pressure distribution under the LPR condition between the base configuration and the case D. From these drawings, it turns out that even under the LPR condition, the non-axisymmetric diffuser forms a more uniform static pressure distribution.

(Note) r : Radius
            r_2 : Diffuser inlet radius

Fig. 14 Distortion index in diffuser at LPR near-surge conditions

(Note) p : Static pressure
            $\bar{p}$: Circumferential mean static pressure
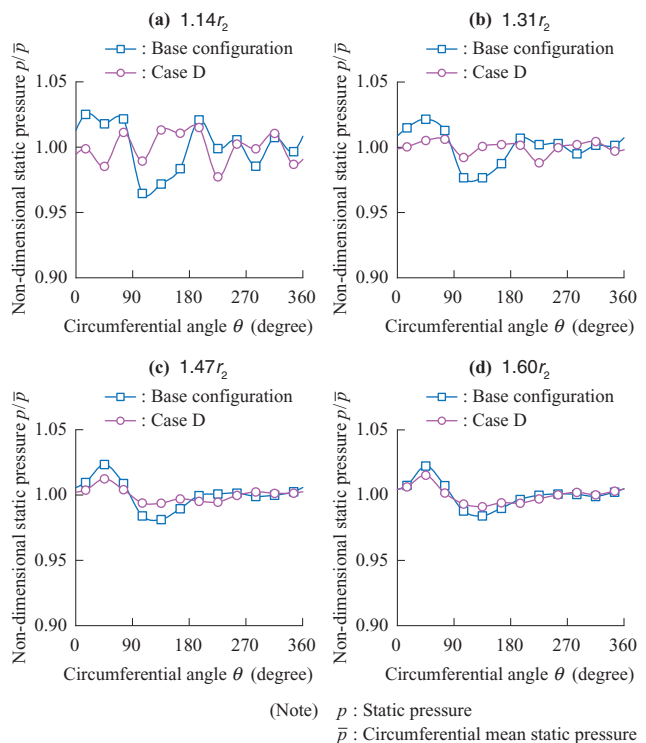
Fig. 15 Circumferential pressure distribution in diffuser at LPR near-surge conditions

4. Experimental results

4.1 Experimental apparatus

In order to confirm the effect of the non-axisymmetric diffuser, the overall performance of the test centrifugal compressor incorporating the non-axisymmetric diffuser was measured. For the experiments, a turbocharger test stand was used. The compressor was driven by a turbine on the same shaft. The rotor speed was adjusted by regulating a turbine flow rate with a valve arranged on the upstream side of the turbine. Also, a compressor flow rate was regulated with a valve arranged on the downstream side of the compressor, and the accuracy of the regulation was approximately 0.007 in unit of the below-described non-dimensional flow rate.

(Note) p : Static pressure
            $\bar{p}$: Circumferential mean static pressure

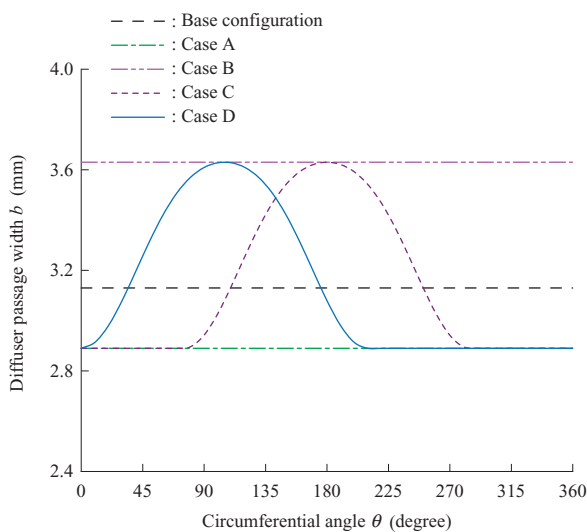**Fig. 13 Circumferential pressure distribution in diffuser at HPR near-surge conditions**

Measurement items were, ① total pressures, static pressures, and total temperatures at the inlet and outlet of the compressor, ② a mass flow rate, ③ a rotor speed, ④ an atmospheric pressure, and ⑤ an atmospheric temperature. The temperatures were measured by thermocouples, and an error was ±1.75°C or less. The pressures were measured by diaphragm pressure gauges, and an error was ±1.25 kPa or less. The mass flow rate was measured by a vortex flowmeter, and a relative error was ±0.5% or less. The rotor speed was measured by an electromagnetic transducer, and a relative error was ±0.25% or less. A relative error in a Stable Flow Range (SFR) defined by the following equation was ±0.8% at the design rotor speed.

$$SFR = \left(\frac{\dot{m}_{\text{choke}} - \dot{m}_{\text{surge}}}{\dot{m}_{\text{choke}}} \right)_{N=\text{const.}} \times 100\% \quad \cdots\cdots (21)$$

$\dot{m}_{\text{choke}}$: Choke flow rate
$\dot{m}_{\text{surge}}$: Surge flow rate
N : Rotor speed

The surge point was determined by making out a change in sound. This is because when the surge occurs, a clear low-frequency periodic sound is heard. In the following, a measurement point where the surge is just on the verge of occurring is referred to as the surge point. The repeatability of the overall performance measurement including the surge point was confirmed by repeating the same measurement twice using the same test compressor of the base configuration[16]. Note that the mass flow rate illustrated in the following figures is made non-dimensional using a common reference value.

Figure 16 illustrates diffuser passage width distributions. The test was performed on diffusers having the five different passage width distributions illustrated in **Fig. 16**. In all the configurations, the same impeller and the same scroll were used. In the base configuration and in the cases A and B, axisymmetric diffusers were respectively used, whereas in the cases C and D, non-axisymmetric diffusers were respectively used. The maximum value of a passage width in the case C is
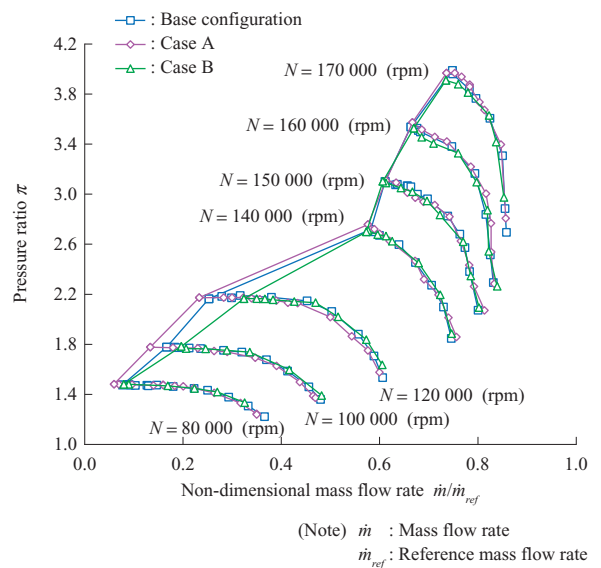
at 180°, which does not conform to the above-described design guideline for non-axisymmetric diffusers. This is to confirm the effectiveness of the design guideline by comparing the case D conforming to the design guideline and the case C not confirming to it.

4.2 Comparison of test results

(1) Comparison among base configuration, case A, and case B

First, **Fig. 17** illustrates the overall performance of the three axisymmetric diffusers (the base configuration and the cases A and B). The performance measurement was carried out at each of seven different rotor speeds. At 140 000 rpm or higher, the three diffusers have almost the same surge flow rate, but at the rotor speeds less than 140 000 rpm, the case A having the smallest passage width exhibits the lowest surge flow rate, whereas the case B having the largest passage width exhibits the highest surge flow rate. Since among these three cases, only the passage width of the diffuser is changed, under such low pressure ratio conditions, a trigger for the surge can be presumed to be the stall of a diffuser. On the other hand, despite such a significant change in passage width (+16% to −8% relative to the base configuration), under the high pressure ratio conditions, neither a surge flow rate nor a choke flow rate exhibits a difference among the three. Accordingly, it can be considered that under such high pressure ratio conditions, the impeller determines both the surge and the choke.

As a result of the above-described comparison among the three cases, it turns out that to stabilize a vaneless diffuser, narrowing a passage width is effective. However, a narrow passage width is not always a good choice. This is because in the case of a narrow passage width, the effect of wall surface friction increases, thus leading to a reduction in efficiency of a compressor. In fact, in the case A having a narrow passage width, the efficiency

Fig. 16 Passage width distribution of diffusers

(Note) $\dot{m}$: Mass flow rate
$\dot{m}_{ref}$: Reference mass flow rate
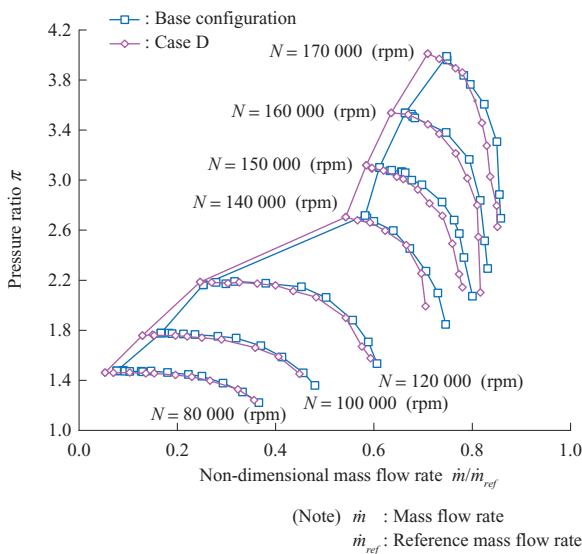
Fig. 17 Overall performance of base, case A and case B

on the lower pressure ratio side is lower than in the other two cases[16].

(2) Comparison between base configuration and case D

Figure 18 illustrates a comparison of overall performance between the base configuration and the case D. In the case D, under both of the high and low pressure ratio conditions, the surge flow rates are smaller, demonstrating that the above-described design guideline for non-axisymmetric diffusers is effective. At the design rotor speed (170 000 rpm), *SFR* is larger by 28% than that in the base configuration. Also, in terms of the passage width, the case D lies between the cases A and B; however, under the high pressure conditions, there is no difference in surge flow rates at all between the case A and the case B, which suggests how the circumferential distribution of a passage width is important for a stable operating range of the compressor.

In the test centrifugal compressor, a choke on a high-speed side occurs in the impeller and not at the throat of the vaneless diffuser. In such a situation, usually, the geometry of the diffuser hardly affects a choke flow rate. In fact, in the cases of the three axisymmetric diffusers, as illustrated in **Fig. 17**, there is no difference in choke flow rates. However, as illustrated in **Fig. 18**, a choke flow rate in the case D is lower than that in the base configuration, and therefore it turns out that the non-axisymmetric diffuser has a possible effect on a choke flow rate of the compressor even when a choke does not occur in the diffuser. This seems to suggest that the non-axisymmetric diffuser affects the effective cross-sectional area of the impeller throat, resulting in a possible change in choke flow rate.

The efficiency at the design rotor speed in the case D is lower than that in the base configuration on the larger flow rate side because in this range, the pressure ratio is also lower. However, in a range around a non-dimensional
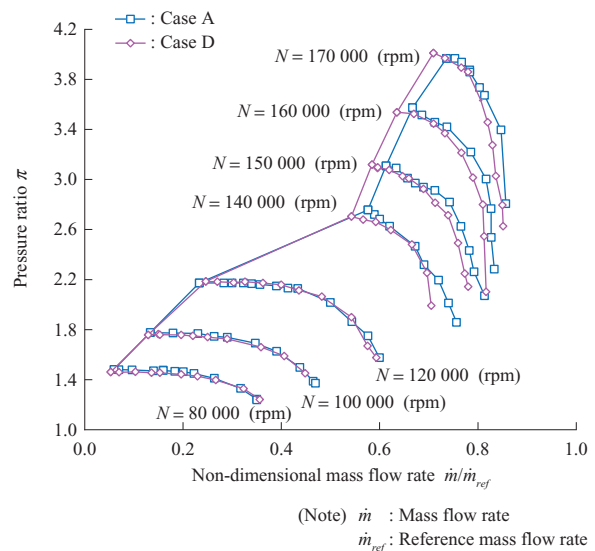
flow rate of 0.8 or less which is often used in actual operations there is no difference in efficiency, and therefore the case D has no practical disadvantage associated with the non-axisymmetry[16].
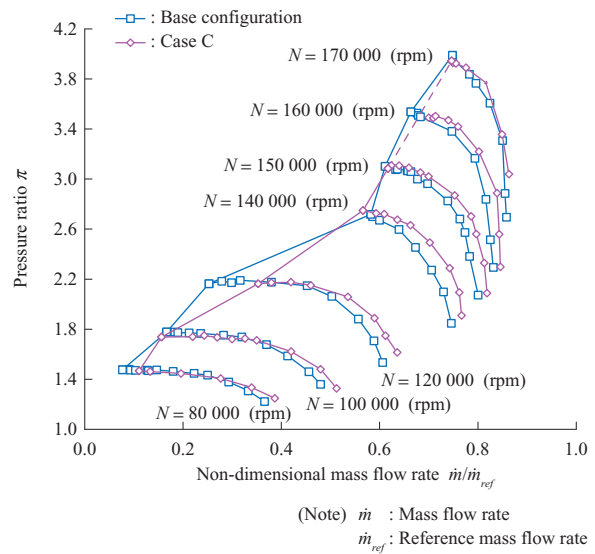
(3) Comparison between case A and case D

Figure 19 illustrates a comparison of overall performance between the cases A and D. The case A corresponds to the axisymmetric diffuser having the smallest passage width. In these two cases, surge lines on the lower rotor speed side are substantially coincident with each other. In these cases, passage widths are the same in an angle range of 210 to 360°, and therefore it can be considered that by narrowing a passage (somewhere) in this angle range, reverse flow in the diffuser can be suppressed to thereby delay a stall.

(4) Comparison between base configuration and case C

Figure 20 illustrates a comparison of overall

(Note) $\dot{m}$: Mass flow rate
$\dot{m}_{ref}$: Reference mass flow rate

Fig. 19 Overall performance of case A and case D

(Note) $\dot{m}$: Mass flow rate
$\dot{m}_{ref}$: Reference mass flow rate

Fig. 18 Overall performance of base and case D

(Note) $\dot{m}$: Mass flow rate
$\dot{m}_{ref}$: Reference mass flow rate

Fig. 20 Overall performance of base and case C

performance between the base configuration and the case C. At 160 000 rpm of the case C, the surge point was not sufficiently clearly identified, and therefore the surge line at around 160 000 rpm is indicated by a dashed line as an estimated line. In the case C, under both of the higher pressure ratio conditions and the lower pressure ratio conditions, surge flow rates are larger. This may be because since the case C does not conform to the proposed design guideline for non-axisymmetric diffusers, the stabilization effect of the non-axisymmetric design is not appropriately obtained. The difference between the cases C and D is only a difference in the circumferential position of the largest passage width, and only by rotating the diffuser of the case D by 75°, the diffuser of the case C can be obtained.

If the geometric non-axisymmetry of a scroll did not impact on compressor performance at all, both were supposed to be completely the same in performance. Therefore, the difference in *SFR* between the two cases clearly indicates that the geometric non-axisymmetry of a scroll significantly affects the stability of a compressor. In addition, although the case C has the same smallest passage width as the axisymmetric case A, on the lower pressure ratio side, the surge flow rates are significantly larger. This makes a marked contrast to the fact that the case D exhibits the same surge flow rates as the case A. It is well understood that to design a non-axisymmetric diffuser, the circumferential phase of a passage width distribution serves as an important factor (when expanding a passage at an inappropriate phase, a surge flow rate increases).

Also, it turns out from **Fig. 20** that the choke flow rates in the case C are larger than in the base configuration, suggesting that the non-axisymmetric diffuser can increase a choke flow rate. However, the mechanism to increase/decrease a choke flow rate of a compressor by a non-axisymmetric diffuser has not been sufficiently understood so far, and further study is required.

5. Conclusion

In the present study, in order to expand a stable operating range of a centrifugal compressor, the vaneless diffuser having a non-axisymmetric passage width distribution has been contrived. As a result, the following conclusions and knowledge have been derived.

(1) Inside an axisymmetric diffuser, a flow field is non-axisymmetric, and under both high and low pressure conditions, the circumferential distribution of static pressure has the minimum value on the downstream side of a scroll tongue. Such pressure distortion tends to be enhanced toward the upstream side of the diffuser. Also, the pressure distortion is more enhanced under a high pressure ratio condition than under a low pressure ratio condition.

(2) The purpose of designing a non-axisymmetric diffuser is to relax the non-axisymmetry of flow inside the diffuser, and to expand (narrow) a passage width at a circumferential phase where static pressure is low (high) is a basic design guideline. This idea is effective for a subsonic flow, and when an impeller outlet flow is supersonic, the trade-off between a supersonic region and a subsonic region is required.

(3) The non-axisymmetric diffuser designed on the basis of the proposed design guideline was incorporated in the test centrifugal compressor and the performance of the diffuser was measured. As a result of the experiments, it turned out that from the low pressure ratio condition to the high pressure ratio condition, the non-axisymmetric diffuser contributed to an improvement in the stability of the compressor. In particular, at the design rotor speed, a stable operating range was expanded by 28% relative to the base configuration.

REFERENCES

(1) T. Elholm, E. Ayder and R. A. Van den Braembussche : Experimental Study of the Swirling Flow in the Volute of a Centrifugal Pump Journal of Turbomachinery Vol. 114 Issue 2 (1992. 4) pp. 366-372

(2) E. Ayder, R. A. Van den Braembussche and J. J. Brasz : Experimental and Theoretical Analysis of the Flow in a Centrifugal Compressor Volute Journal of Turbomachinery Vol. 115 Issue 3 (1993. 7) pp. 582-589

(3) K. Hillewaert and R. A. Van den Braembussche : Numerical simulation of Impeller-Volute Interaction in Centrifugal Compressors Journal of Turbomachinery Vol. 121 Issue 3 (1999. 7) pp. 603-608

(4) A. Reunanen, H. Pitkänen, T. Siikonen, H. Heiska, J. Larjola, H. Esa and P. Sallinen : Computational and Experimental Comparison of Different Volute Geometries in a Radial Compressor ASME Proceedings Turbomachinery Paper No. 2000-GT-469 (2000. 5) pp. V001T03A040

(5) J. M. Sorokes, C. J. Borer and J. M. Koch : Investigation of the Circumferential Static Pressure Non-Uniformity Caused by a Centrifugal Compressor Discharge Volute ASME Paper No. 98-GT-326 (1998. 6) pp. V001T01A088

(6) A. Fatsis, S. Pierret and R. A. Van den Braembussche : Three-Dimensional Unsteady Flow and Forces in Centrifugal Impellers With Circumferential Distortion of the Outlet Static Pressure Journal of Turbomachinery Vol. 119 Issue 1 (1997. 1) pp. 94-102

(7) F. H. Gu and A. Engeda : A Numerical Investigation on the Volute/Impeller Steady-State Interaction Due to Circumferential Distortion ASME Proceedings Turbomachinery Paper No. 2001-GT-0328 (2001. 6) pp. V001T03A030

(8) F. H. Gu, A. Engeda, M. Cave and J. L. D. Liberti : A Numerical Investigation on the Volute/Diffuser Interaction Due to the Axial Distortion at the Impeller Exit Journal of Fluids Engineering Vol. 123 Issue 3 (2001. 4) pp. 475-483

(9) M. Yang, X. Zheng, Y. Zhang, T. Bamba, H. Tamaki, J. Huenteler, and Z. Li : Stability Improvement of High-Pressure-Ratio Turbocharger Centrifugal Compressor by Asymmetric Flow Control - Part I: Non-Axisymmetric Flow in Centrifugal Compressor   ASME Proceedings Turbomachinery Paper No. GT2010-22581 (2010. 6) pp. 1 891-1 902

(10) X. Q. Zheng, J. Huenteler, M. Y. Yang, Y. J. Zhang and T. Bamba : Influence of the Volute on the Flow in a Centrifugal Compressor of a High-Pressure Ratio Turbocharger Proceedings of the Institution of Mechanical Engineers Part A   Journal of Power and Energy Vol. 224 (2010)   pp. 1 157-1 169

(11) Y. Lin, X. Zheng, L. Jin, H. Tamaki and T. Kawakubo : A Novel Experimental Method to Evaluate the Impact of the Volute's Asymmetry on the Performance of a High Pressure Ratio Turbocharger Compressor   Science China - Series E Technological Sciences Vol. 55 (2012) pp. 1 695-1 700

(12) J. M. Sorokes and J. M. Koch : The Influence of Low Solidity Vaned Diffusers on the Static Pressure Non-Uniformity Caused by a Centrifugal Compressor Discharge Volute   ASME Proceedings Turbomachinery Paper No. 2000-GT-0454 (2000. 5)   pp. V001T03A028

(13) C. Xu and R. Amano : Eliminating Static Pressure Distortion by a Large Cut Back Tongue Volute   ASME Proceedings Microturbines and Small Turbomachinery Paper No. GT2006-90001 (2006. 5)   pp. 155-164

(14) C. Xu and M. Müller : Development and Design of a Centrifugal Compressor Volute   International Journal of Rotating Machinery Vol. 3 Issue 3 (2005. 4)   pp. 190-196

(15) X. Zheng, Y. Zhang, M. Yang, T. Bamba and H. Tamaki : Stability Improvement of High-Pressure-Ratio Turbocharger Centrifugal Compressor by Asymmetric Flow Control - Part II : Non-Axisymmetric Self Recirculation Casing Treatment   ASME Proceedings Turbomachinery Paper No. GT2010-22582 (2010. 6) pp. 1 903-1 912

(16) X. Zheng. Y. Lin, W. Zhuge, Y. Zhang, H. Tamaki and T. Kawakubo : Stability Improvement of Turbocharger Centrifugal Compressor by Asymmetric Vaneless Diffuser Treatment   ASME Proceedings Radial Turbomachinery Aerodynamics Paper No. GT2013-94705 (2013. 6) pp. V06CT40A006

(17) D. Japikse : Advanced Diffusion Levels in Turbocharger Compressors and Component Matching   Proc. First International Conference on Turbocharging and Turbochargers IMechE (1982)   pp. 143-156

(18) H. W. Iversen, R. E. Rolling and J. J. Carlson : Volute Pressure Distribution, Radial Force on the Impeller, and Volute Mixing Losses of a Radial Flow Centrifugal Pump   ASME Journal of Engineering for Power Vol. 82 Issue 2 (1960. 4)   pp. 136-143

(19) G. Chochua, J. M. Koch and J. M. Sorokes : Analytical and Computational Study of Radial Loads in Volutes and Collectors   ASME Proceedings Turbomachinery Paper No. GT2005-68822 (2005. 6) pp. 871-879

(20) E. M. Greitzer, C. S. Tan and M. B. Graf : Internal Flow : Concepts and Applications   Cambridge University Press (2007. 5) pp. 51-54

(21) W. Jansen : Rotating Stall in a Radial Vaneless Diffuser   Journal of Basic Engineering Vol. 86 Issue 4 (1965. 12) pp. 750-758